# Magmatic Epidote and Amphibole from the Rio Espinharas Hybrid Complex, Northeastern Brazil

THOMAS F. C. CAMPOS[1], ANA MARGARIDA R. NEIVA, LAURO VALENTIM STOLL NARDI[3],
LUCIANO SCHAEFFER PEREIRA[4]; LEONARDO FRAGA BONZANINI[4],
REINALDO A. PETTA[1], FRANZ MICHAEL MEYER[5]

1. Department of Geology of Federal University of Rio Grande do Norte, 59072-970 Natal RN, Brazil. e-mail : tcampos@geologia.ufrn.br;
2. Department of Earth Sciences, University of Coimbra, 3000-272 Coimbra, Portugal;
3. Institute of Geosciences, Federal University of Rio Grande do Sul, 91501-970 Porto Alegre, RS, Brazil;
4. Geosciences Pos-graduation Program,   Federal University of Rio Grande do Norte Brazil;
5. Geology Institute (RWTH) Aachen, Germany.

**Abstract**-  The petrography and chemistry of epidote and amphibole from the Rio Espinharas hybrid complex (REHC), northeastern Brazil are reported. The Rio Espinharas complex is composed of an intimate association of diorite to shoshonitic metaluminous quartzmonzonite to slightly peraluminous syenogranite. The epidote shows four textural relationships: three are primary and one is resulting from sub-solidus reaction. Euhedral epidote is dispersed and associated mainly with biotite and amphibole. In some cases euhedral crystals of the epidote contain allanite cores, which are subhedral to anhedral and constitute in average less than 20% of the whole grain. The contact between primary epidote and plagioclase is corroded, suggesting reaction with the host-magma. Secondary anhedral epidote is rare and results from plagioclase alteration. The preservation of magmatic epidote in granitic rocks emplaced in the upper crust is attributed to rapid magma ascent, which implies fast upward transport probably by dyking associated to shear zone. The REHC occurs between two transcurrent faults that impose an elongated shape, suggesting that magma filled fractures. The time of 14 years required for dissolution zones of 0.15 mm width of epidote on porphyritic quartz monzonite, corresponds to an average ascent rate of $\geq$ 700 m year$^{-1}$ from 7.1 to 2.9 kbar.

**Keywords**- magmatic epidote, amphibole, Neoproterozoic granite, mineral chemistry.

## INTRODUCTION

The existence of magmatic epidote is known since the end of the 19$^{th}$ century (Hobbs, 1889; Keyes, 1893; Cornelius, 1915), even though its petrogenetic importance was only recognized about one hundred years later by Zen & Hammarstrom (1984). They identified the epidote as an important magmatic phase in the calc-alkaline granites of the North American Cordillera, where it only appears in intrusions crystallized under medium- and high-pressure. These same authors, based upon the experimental data of Naney (1983), estimated a minimum pressure of crystallization for epidote of about 6 to 8 kbar; which is in accordance with the minimum pressure of 6 kbar suggested by Liou (1973) and Crawford & Hollister (1982). This minimum pressure was questioned by Moench (1985), since he found magmatic epidote in several granite intrusions, whose pressures estimated from the aureoles of contact metamorphism, were about 4

kbar. Brandon *et al.* (1996) and Schmidt & Thompson (1996) reported experiments which suggest that magmatic epidote can be preserved under pressures lower than 4 kbar, which is due to: (i) a fast ascension of the magma that prevents a complete dissolution of epidote crystals, or to (ii) magmatic crystallization at water-saturated and strongly oxidizing conditions (hematite-magnetite buffer) that expands the magmatic stability field of epidote down to pressures of 3 kbar. For less oxidizing (NNO buffer) conditions the minimum pressure were found to be 4.5 kbar.

The magmatic stage in which epidote crystallizes remains controversial, and there are evidences indicating that magmatic epidote can crystallize close to solidus temperatures, and that it is probably formed through the reaction of hornblende + plagioclase + magnetite with hydrous magma, generating epidote + biotite + quartz (Naney, 1983; Zen & Hammarstron, 1984; Schmidt & Thompson, 1996, Schimdt & Poli, 2004).

However, the existence of epidote phenocrysts in hornblende-free dacite dykes suggests that the presence of amphibole is not necessary for the generation of magmatic epidote, and that magmatic epidote can be an early crystallized phase (Zen & Hammarstron, 1984; Evans & Vances, 1987; Dawes & Evans, 1991). According to Tulloch (1979, 1986); Naney (1983); Zen & Hammarstrom (1984; 1988); Zen (1985); Johnston & Wyllie (1988); Bellieni *et al.* (1991); and Vyhnal *et al.* (1991), the pistacite component of the epidote [Ps = $Fe^{3+}$ / ($Fe^{3+}$ +$Al^{IV}$)] can be used to identify magmatic epidote (with Ps ranging from 20 to 30%), and discriminate it from secondary epidote, produced from sub-solidus alterations. Epidote originating from plagioclase alteration shows Ps ranging from 0 to 20%, and that derived from biotite alteration has 30 to 50%. According to these authors, magmatic epidote generally occurs as: euhedral crystals, with or without compositional zoning and/or allanite core, frequently in contact or involved by aggregates of biotite, and sometimes of quartz or K–feldspar. The euhedral crystals when in contact with plagioclase show intergrowths (worm-like type), which are interpreted as product of melt dissolution (Brandon *et al.*, 1996). The existence of euhedral epidote dispersed in the groundmass suggests a direct crystallization from liquid rather than a product of amphibole re–absorption in the melt (Zen & Hammarstrom, 1984). These criteria were criticized by Keane and Morrison (1997), based on data from combined analysis of oxygen isotopes by laser microprobe in epidote, plagioclase and zircon crystals from the hornblende quartz–monzonite of San Gabriel mountains (California–USA). They identified epidote, with values of $\delta^{18}O > 5$ ‰, to be of magmatic origin, and these values appear both in euhedral and anhedral grains. They also demonstrated that euhedral crystals, when in contact with biotite, can have values of $\delta^{18}O$ lower than 5 ‰, which are typical of sub-solidus products. Keane and Morrison (1997) also showed that intra–crystalline $\delta^{18}O$ contents can vary from typical magmatic to the sub–solidus compositions, which suggests chemical adjustment of the individual epidote crystals concomitantly with the modifications of the system.

The subject of this paper is to document the existence of primary epidote in the Precambrian metaluminous to peraluminous shoshonitic granitoids from the Rio Espinharas hybrid complex, in the Central Domain of Borborema Province, northeastern Brazil (Fig.1). This study complements the pioneer works of Tulloch (1986), Sial (1990), Bellieni *et al.* (1991), Sial *et al.* (1997, 1999) and Toselli *et al.* (1997), who reported the existence of primary epidote in granitoids outside North America. The epidote textural relations and the estimated physical and chemical conditions of its formation, combined with the Al–in–hornblende barometer and thermometer, were used in order to interpret the conditions prevailing during the crystallization of Rio Espinharas hybrid complex.

## ANALYTICAL METHODS

Major and trace elements of rocks were determined by X-ray fluorescence (XRF) at the Department of Earth Sciences, University of Manchester, UK, using the method of Brown *et al.* (1973). A precision of ± 1% was obtained for major elements and Rb, and ± 4% for other trace elements. The chemical analyses of minerals were determined with a modified Cambridge Geoscan energy-dispersive system at Manchester University with precision of ± 5% and complementary microprobe analyses were realized at Aachen University of Technology (RWTH), Germany and Mining and Geological Institute of Portugal. FeO of rocks and amphibole were determined at the Department of Earth Sciences, Coimbra University, Portugal, by titration with standardized potassium permanganate solution, with precision of ± 1%.

## GEOLOGY AND GEOCHEMISTRY OF THE RIO ESPINHARAS HYBRID COMPLEX

The Rio Espinharas hybrid complex is intruded in a low–stress zone, limited by two oblique transcurrent shear zones of general NNE–SSW direction (Fig.1a). It is composed of porphyritic and non–porphyritic shoshonitic metaluminous quartz monzonite associated with metaluminous peraluminous syenogranite (Fig.1b). Minor amounts of diorite, quartz monzodiorite and quartz syenite, also occur, but these last two rocks can not be represented at the scale of figure 1b, both contain some dioritic enclaves. These granitoids have diffuse and interpenetrated contacts (Campos, 1997; Campos *et al.* 2002). Quartz monzonites contain more amphibole (≈20%) than biotite (≈15%), and epidote is present in lower amounts (<0.15%) than other accessory minerals such as titanite, magnetite, zircon and allanite. Amphibole, pyroxene, biotite and plagioclase have compositions

and chemical zoning which are typically magmatic with no evidence of post–magmatic alteration. The absence of chlorite and the fresh appearance of plagioclase, also rule out a subsolidus high–temperature or a retrograde greenschist–facies overprint, and consequently excluded the occurrence of subsolidus epidote. The pluton intruded into biotite–amphibole augen gneisses of amphibolite facies, and the contact between them is sharp and discordant, with no distinguishable contact metamorphism and deformation (Gonzalez, 1984).
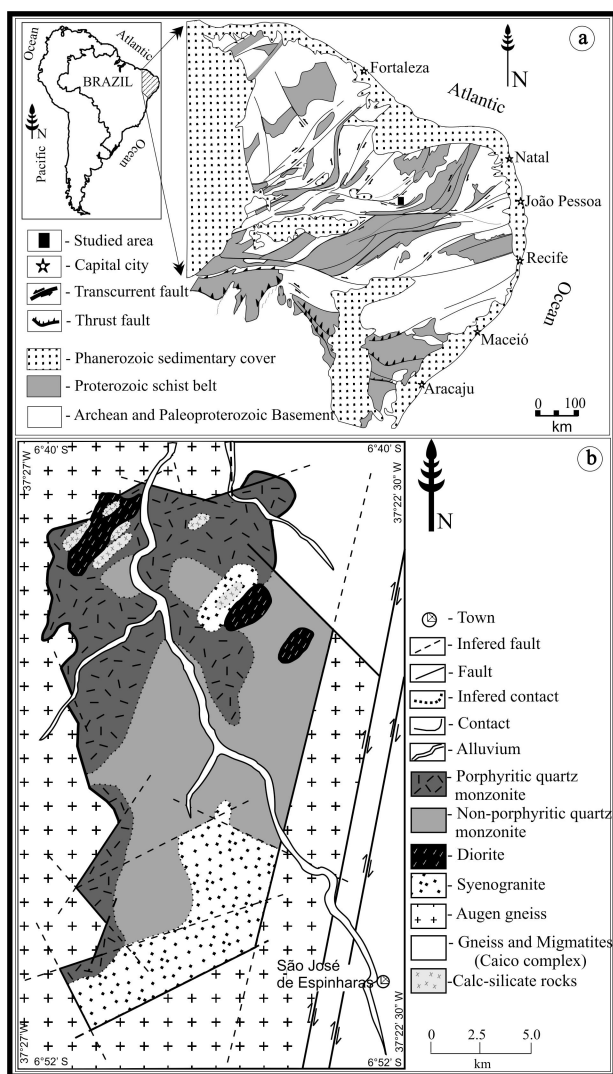


Figure 1– a) Location of the Borborema Province and Serido region in northeastern Brazil; b) Generalized geological map of Borborema province based on Jardim de Sá (1994). b) Geological map of the Rio Espinharas hybrid complex, northeastern Brazil based on Campos et al. (2002).

The Rio Espinharas hybrid complex displays a large chemical spectrum, from diorite to granite (SiO$_2$: 47.8–77.0 wt. % and MgO: 9.2–0.1 wt. %) and is illustrated in figure 2. The Fe + Mg + Ti parameter, calculated as milications of the elements,

is proportional to the mafic mineral contents of the rocks (Dias & Leterrier, 1994), and was used here as a differentiation index. Linear trends without any significant gap are observed in most major and trace element variation diagrams suggesting that quartz–monzonite, porphyritic quartz–monzonite, quartz–monzodiorite and quartz–syenite are hybrid rocks (Campos, 1997; Campos et al. 2002 and reference therein) predominantly resulting from variable degrees of mixing between the dioritic and the syenogranitic magmas (Fig.2). Mixing process is also supported by the initial ($^{87}$Sr/$^{86}$Sr)$_{initial}$, calculated for the age of 601 Ma, yielded by the syenogranite errochron calculated for quartz–monzonite (0.7083-0.7092), porphyritic quartz–monzonite (0.7078-0.7082), quartz–monzodiorite (0.7086) and quartz–syenite (0.7077), that range between those for diorite (0.7064) and syenogranite (0.7075-0.7088), and are closer to those for syenogranite, and by the errochron formed by these rocks (Campos, 1997; Campos et al. 2002). However, the bell–shaped concave–downward curves with scatter for Sr, Ba and Zr overcast the magmatic evolution these rocks (Fig.2). The two step evolution for these elements can be explained as a result of two trends in each diagram: (i) a mixing line represented by the rocks ranging from diorite to syenogranite end-members, which define a positive linear trend; and (ii) a fractional crystallization trend represented by the negative linear trend showed by the syenogranite and micro-syenogranite. Syenogranite and microsyenogranite are interpreted as representing two different pulses of granite magma, although the composition of some samples overlap and the negative trends may correspond to a fractional crystallization process better defined in the syenogranite samples (Campos, 1997; Campos et al. 2002 and reference therein).

According to geochemical arguments by Campos (1997) and Campos et al. (2002) the syenogranite is of anatectic origin, generated by partial melting of upper continental crust, probably promoted by underplate of an upper mantlederived magma, which supplied the necessary heat to induce melting. The geochemical signature of the diorite is consistent with its derivation from an enriched mantle source. The syenogranite and the diorite seem to represent the endmembers, while the quartz–monzonite, quartz–monzodiorite, quartz–syenite and dioritic enclaves would be hybrid products, which resulted from mixing of the two end–members at deeper levels than the final level of magma emplacement, with a probable minor contri-
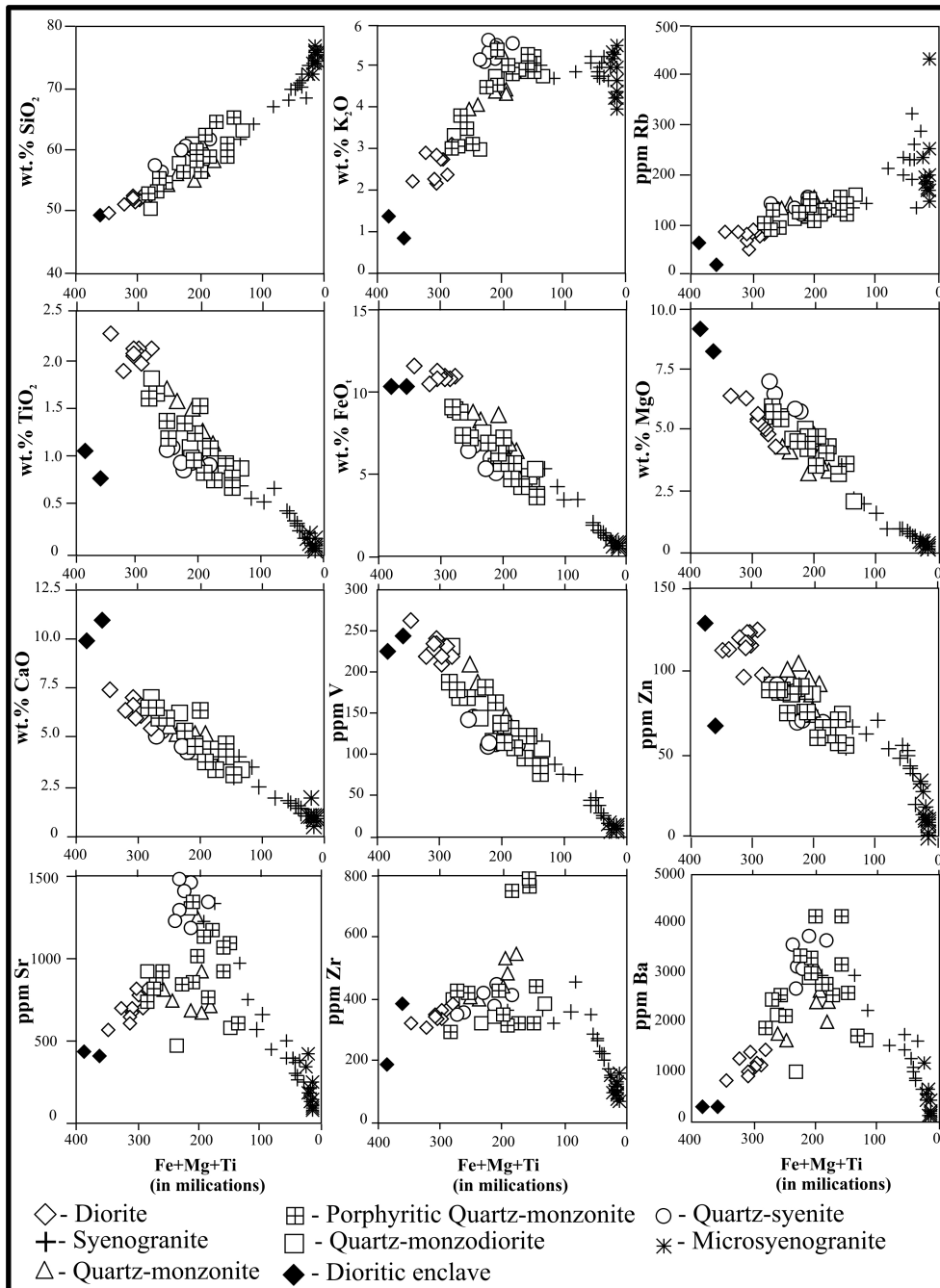
Figure 2– Variation diagrams of selected major and trace elements of plutonic rocks from Rio Espinharas hybrid complex, northeastern Brazil. The (Fe+Mg+Ti) milications parameter was used here as a differentiation index (Dias & Leterrier, 1994).

bution of mineral fractionation. The age of 601 ± 29 Ma and a initial $(^{87}Sr/^{86}Sr)_0$ ratio of 0.7083 ± 0.0003 of the syenogranite are within the range of other Brasiliano (Pan-African) granitoids in the Serido Belt of the Borborema Province (Campos, 1997; Campos et al. 2002).

## AMPHIBOLE PETROGRAPHY AND CHEMISTRY

Selected amphibole rim compositions of am-

phibole of granitoids from Rio Espinharas hybrid complex are listed in table 1. The chemical classification of these amphiboles is based on Leake et al. (1997), and the chemical classifications (Fig.3a) correspond to ferro–edenite, edenite, ferro-pargasite, magnesiohastingsite, ferrotschermakite, tschermakite, magnesiohornblende, and actinolite (Campos, 1997; Campos et al. 2002 and reference therein). There are continuous, systematic and no concentric variations from Fe–rich core to Mg–rich rim, and in general, they show lower Si and Ca+Na+K contents

(Fig.3b) typical for magmatic amphibole (Leake, 1971). Rare crystals of ferro-hornblende, edenite or ferro–edenite, and magnesio-hornblende show discrete enrichment in Mg and Si towards the rims, which suggest a reaction between amphibole phenocrysts and the magma (e.g. Yamaguchi, 1985; Pe-Piper, 1988). In general, amphibole crystals have uniform composition, but some grains have isolated and randomly distributed magnesian-rich domains. These Mg- and Si-enriched patchy domains reflect the adjustment of amphibole to magmatic changes where some parts of the grain were more reactive with the magma than others, similar to amphiboles from Finnmarka granodiorite studied by Czamanske & Wones (1973).

In general, no relationship was found between crystalographic orientation and chemical composition, since most amphibole crystals can be heterogeneous on the scale of a single thin section (Fig.4) (e.g. Robinson *et al.*, 1971; Droop, 1994). There is no textural evidence for actinolite to be derived from late hydrothermal alteration, and it is

Table 1– Selected amphibole rim compositions (wt. %) of amphibole of plutonic rocks from the Rio Espinharas hybrid complex, northeastern Brazil.

| | Syenogranite | | | Diorite | | | Dioritic enclaves | | |
|---|---|---|---|---|---|---|---|---|---|
| | Fe-hbl | Ed | Fe-ts | Fe-ed | Fe-ts | Fe-ed | Fe-hbl | Mg-hs | Ts |
| $SiO_2$ | 42,87 | 47,41 | 42,65 | 43,48 | 42,37 | 45,86 | 42,46 | 41,16 | 43,38 |
| $TiO_2$ | 0,20 | 0,77 | 1,05 | 0,66 | 0,51 | 0,37 | 0,76 | 1,88 | 1,73 |
| $Al_2O_3$ | 9,16 | 6,49 | 10,36 | 9,67 | 10,57 | 10,76 | 10,30 | 11,72 | 11,10 |
| $Cr_2O_3$ | 0,01 | 0,13 | 0,01 | 0,08 | 0,05 | 0,01 | 0,01 | 0,03 | 0,08 |
| FeO | 21,22 | 16,54 | 21,83 | 21,75 | 22,55 | 17,62 | 22,34 | 17,96 | 17,47 |
| MnO | 0,06 | 0,04 | 0,03 | 0,02 | 0,01 | 0,01 | 0,02 | 0,05 | 0,02 |
| MgO | 8,74 | 12,43 | 8,03 | 8,12 | 7,29 | 8,46 | 6,88 | 10,87 | 10,11 |
| CaO | 11,40 | 11,82 | 11,46 | 11,84 | 11,51 | 11,46 | 11,46 | 10,45 | 11,87 |
| $Na_2O$ | 1,72 | 1,49 | 1,34 | 1,63 | 1,53 | 1,49 | 1,49 | 1,83 | 1,59 |
| $K_2O$ | 1,43 | 0,71 | 1,25 | 0,91 | 0,89 | 1,02 | 1,02 | 2,37 | 1,09 |
| Total | 96,81 | 97,83 | 98,01 | 98,16 | 97,28 | 97,06 | 96,74 | 98,32 | 98,44 |

*Structural formulae calculated by the method of Schumacher (1991; 1997).*

| | | | | | | | | | |
|---|---|---|---|---|---|---|---|---|---|
| Si | 6,534 | 6,978 | 6,478 | 6,514 | 6,496 | 6,877 | 6,563 | 6,009 | 6,442 |
| $Al^{IV}$ | 1,466 | 1,022 | 1,522 | 1,486 | 1,504 | 1,123 | 1,437 | 1,991 | 1,558 |
| *T* | *8,00* | *8,00* | *8,00* | *8,00* | *8,00* | *8,00* | *8,00* | *8,00* | *8,00* |
| $Al^{VI}$ | 0,180 | 0,103 | 0,332 | 0,221 | 0,407 | 0,779 | 0,439 | 0,025 | 0,385 |
| $Ti^{VI}$ | 0,023 | 0,085 | 0,120 | 0,074 | 0,059 | 0,042 | 0,088 | 0,206 | 0,193 |
| $Fe^{+3}$ | 0,925 | 2,727 | 0,484 | 1,814 | 0,501 | 1,891 | 0,366 | 2,366 | 0,341 |
| Cr | 0,001 | 0,015 | 0,001 | 0,009 | 0,006 | 0,001 | 0,001 | 0,003 | 0,009 |
| Mg | 1,986 | 2,069 | 1,818 | 1,814 | 1,666 | 1,891 | 1,585 | 2,366 | 2,238 |
| $Fe^{+2}$ | 1,780 | — | 2,244 | 1,068 | 2,361 | 0,395 | 2,519 | 0,033 | 1,828 |
| Mn | 0,008 | — | — | — | — | — | — | — | 0,003 |
| | *4,90* | *5,00* | *5,00* | *5,00* | *5,00* | *5,00* | *5,00* | *5,00* | *5,00* |
| Mg | 0,000 | 0,658 | 0,000 | — | — | — | — | — | — |
| $Fe^{+2}$ | 0,000 | 1,532 | 0,045 | 0,691 | 0,029 | 1,715 | 0,002 | 0,439 | — |
| Mn | 0,000 | 0,005 | 0,004 | 0,003 | 0,001 | 0,001 | 0,003 | 0,006 | — |
| Ca | 1,862 | 1,864 | 1,865 | 1,900 | 1,891 | 1,841 | 1,898 | 1,635 | 1,889 |
| Na | 0,138 | — | 0,086 | — | 0,079 | — | 0,097 | — | 0,111 |
| | *2,00* | *4,06* | *2,00* | *2,59* | *2,00* | *3,56* | *2,00* | *2,08* | *2,00* |
| Na | 0,370 | 0,425 | 0,308 | 0,473 | 0,376 | 0,433 | 0,349 | 0,518 | 0,346 |
| K | 0,278 | 0,133 | 0,242 | 0,174 | 0,174 | 0,195 | 0,201 | 0,441 | 0,206 |
| | *0,648* | *0,558* | *0,550* | *0,647* | *0,550* | *0,628* | *0,550* | *0,959* | *0,553* |
| Mg# | 0,53 | 0,49 | 0,44 | 0,51 | 0,41 | 0,47 | 0,39 | 0,83 | 0,55 |

Ed - edenite, Fe-ed - ferro-edenite, Mg-hbl - magnesiohornblende, Fe-ts – ferrotschermakite, Mg-hs – magnesio-hastingite, Fe-hbl - ferrohornblende, Fe-prg - ferropargasite, Fe-ts – ferrotschermakite.

Table 1– Cont.

| Quartzmonzonite | | | Porphyritic quartzmonzonite | | | | Quartzmonzodiorite | | | Quartzsyenite | |
|---|---|---|---|---|---|---|---|---|---|---|---|
| Fe-prg | Fe-hbl | Ed | Fe-hbl | Fe-prg | Ts | Fe-ed | Mg-hbl | Fe-ed | Fe-ts | Ed | Mg-hbl |
| 42,97 | 42,66 | 43,83 | 43,09 | 41,83 | 42,15 | 43,65 | 43,04 | 43,05 | 42,54 | 47,56 | 46,56 |
| 0,93 | 0,94 | 0,68 | 0,94 | 0,35 | 1,35 | 1,51 | 1,08 | 1,36 | 1,68 | 1,25 | 1,25 |
| 10,22 | 10,51 | 10,58 | 10,15 | 11,32 | 9,82 | 9,45 | 9,39 | 9,26 | 9,30 | 6,84 | 6,84 |
| 0,01 | 0,02 | 0,07 | 0,03 | 0,01 | 0,06 | 0,01 | 0,06 | 0,07 | 0,06 | 0,12 | 0,12 |
| 21,41 | 21,11 | 20,28 | 22,28 | 22,49 | 19,28 | 21,17 | 20,49 | 21,81 | 21,64 | 15,24 | 15,24 |
| 0,34 | 0,15 | 0,24 | 0,10 | 0,39 | 0,13 | 0,34 | 0,04 | 0,04 | 0,05 | 0,09 | 0,09 |
| 7,83 | 8,55 | 8,86 | 7,18 | 7,28 | 9,26 | 8,27 | 9,07 | 8,14 | 8,58 | 12,88 | 12,88 |
| 11,49 | 11,70 | 11,76 | 11,38 | 11,79 | 11,46 | 11,56 | 11,52 | 11,42 | 11,40 | 11,55 | 11,55 |
| 1,32 | 1,52 | 1,34 | 1,54 | 1,28 | 1,81 | 1,30 | 1,71 | 1,61 | 1,61 | 1,88 | 1,88 |
| 1,28 | 1,22 | 1,03 | 1,25 | 1,34 | 1,24 | 1,20 | 1,16 | 1,13 | 1,14 | 0,74 | 0,74 |
| 97,80 | 98,38 | 98,67 | 97,94 | 98,08 | 96,56 | 98,46 | 97,56 | 97,89 | 98,00 | 98,15 | 97,15 |

*Structural formulae calculated by the method of Schumacher (1991; 1997).*

| | | | | | | | | | | | |
|---|---|---|---|---|---|---|---|---|---|---|---|
| 6,479 | 6,563 | 6,503 | 6,571 | 6,297 | 6,414 | 6,543 | 6,511 | 6,507 | 6,452 | 6,999 | 6,919 |
| 1,521 | 1,437 | 1,497 | 1,429 | 1,703 | 1,586 | 1,457 | 1,489 | 1,493 | 1,548 | 1,001 | 1,081 |
| *8,00* | *8,00* | *8,00* | *8,00* | *8,00* | *8,00* | *8,00* | *8,00* | *8,00* | *8,00* | *8,00* | *8,00* |
| 0,296 | 0,439 | 0,353 | 0,396 | 0,306 | 0,175 | 0,213 | 0,185 | 0,157 | 0,114 | 0,185 | 0,117 |
| 0,105 | 0,088 | 0,076 | 0,108 | 0,040 | 0,154 | 0,170 | 0,123 | 0,155 | 0,192 | 0,138 | 0,140 |
| 1,760 | 0,366 | 1,960 | 0,411 | 1,634 | 0,769 | 1,848 | 0,676 | 0,798 | 0,637 | 0,107 | 0,252 |
| 0,001 | 0,001 | 0,008 | 0,004 | 0,001 | 0,007 | 0,001 | 0,007 | 0,008 | 0,007 | 0,014 | 0,014 |
| 1,760 | 1,585 | 1,960 | 1,632 | 1,634 | 2,101 | 1,848 | 2,045 | 1,834 | 1,940 | 2,826 | 2,853 |
| 1,078 | 2,519 | 0,643 | 2,430 | 1,386 | 1,684 | 0,919 | 1,916 | 1,959 | 2,108 | 1,729 | 1,624 |
| — | — | — | 0,013 | — | 0,017 | — | 0,005 | 0,005 | 0,002 | — | — |
| *5,00* | *5,00* | *5,00* | *4,99* | *5,00* | *4,91* | *5,00* | *4,96* | *4,92* | *5,00* | *5,00* | *5,00* |
| — | — | — | — | — | — | — | — | — | — | — | — |
| 0,765 | 0,002 | 1,098 | — | 0,286 | — | 1,014 | — | — | — | 0,039 | 0,018 |
| 0,043 | 0,003 | 0,030 | — | 0,050 | — | 0,043 | — | — | 0,004 | 0,011 | 0,011 |
| 1,856 | 1,898 | 1,870 | 1,859 | 1,902 | 1,868 | 1,857 | 1,867 | 1,849 | 1,852 | 1,821 | 1,839 |
| — | 0,097 | — | 0,141 | — | 0,132 | — | 0,133 | 0,151 | 0,144 | 0,129 | 0,132 |
| *2,66* | *2,00* | *3,00* | *2,00* | *2,24* | *2,00* | *2,91* | *2,00* | *2,00* | *2,00* | *2,00* | *2,00* |
| 0,386 | 0,349 | 0,385 | 0,313 | 0,374 | 0,402 | 0,378 | 0,369 | 0,321 | 0,330 | 0,408 | 0,410 |
| 0,246 | 0,201 | 0,195 | 0,243 | 0,257 | 0,241 | 0,229 | 0,224 | 0,218 | 0,221 | 0,139 | 0,140 |
| *0,632* | *0,550* | *0,580* | *0,556* | *0,631* | *0,643* | *0,607* | *0,593* | *0,539* | *0,550* | *0,547* | *0,550* |
| 0,49 | 0,39 | 0,53 | 0,40 | 0,49 | 0,56 | 0,49 | 0,52 | 0,48 | 0,48 | 0,62 | 0,64 |

Ed - edenite, Fe-ed - ferro-edenite, Mg-hbl - magnesiohornblende, Fe-ts – ferrotschermakite, Mg-hs - magnesiohastingite, Fe-hbl - ferrohornblende, Fe-prg - ferropargasite, Fe-ts – ferrotschermakite.

not associated with crystal edges, fractures and veins and some actinolite and homogeneous hornblende form clots at the expense of clinopyroxene, with sharp contact between them. Consequently, a few crystals with an irregular core of actinolite and a homogeneous rim of ferro–edenite suggests pyroxene re-equilibrated with the melt to form calcic amphibole, and the thin actinolite rims on clinopyroxene are thought to represent incomplete reaction products of clinopyroxene + melt ⇒ actinolite ⇒ ferro-edenite or magnesiohornblende. The composite corona of thin actinolite inner rims and with more external rims of homogeneous ferro–edenite or magnesiohornblende that mantled the few irregular or skeletal diopside cores shows similar composition to the simple amphibole crystals from elsewhere in the hybrid complex studied here, despite the fact that shows similar texture and composition as well to amphibole of the mafic rocks of the Jeffers Brook plutonic complex from Nova Scotia (Pe-Piper, 1988).

For simplicity in subsequent discussion, all

amphiboles are referred to as hornblende. In general, the hornblende is characterized by decrease in Mg and regular increase in total Al, $Fe^{2+}$, $Fe^{2+}/(Fe^{2+}+Mg)$, K and $[Na+K]_{(A)}$ with an increase in Si (Campos, 1997; Campos *et al.*, 2002 and reference therein). These amphibole show a regular
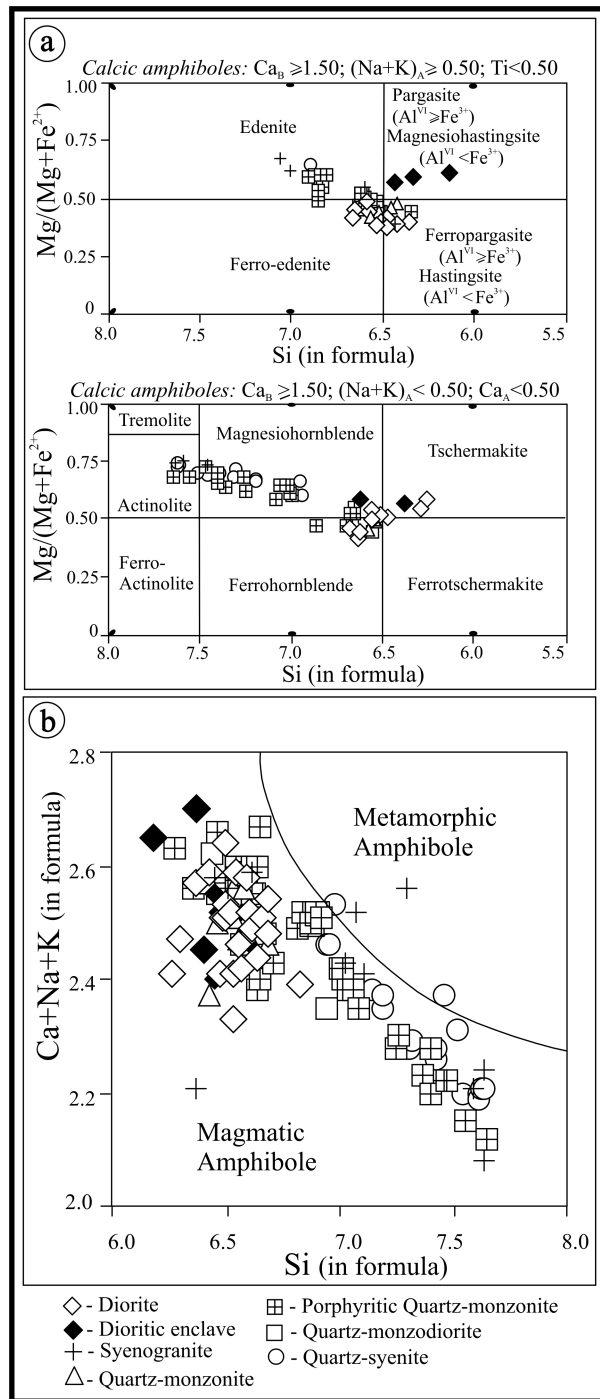


Figure 4– a) Amphibole crystals from quartz monzonite (XPL). Note the twined amphibole crystals and acicular apatite; b) Magnesiohornblende with quartz inclusions from porphyritic quartz monzonite. Epidote is not visible in these sections. Hbl: amphibole; Qz: quartz; Bt: biotite; Apt: apatite. Mineral abbreviation based on Kretz (1983). XPL: cross-polarized light.

increase in $[Na+K]_{(A)}$ with an increase in total Al and decrease in $Al^{IV}$ with increase in $Mg/(Mg+Fe^{2+})$ (Fig.5). The hornblende of dioritic enclaves is depleted in total $Fe^{2+}$, $Fe^{2+}/(Fe^{2+}+Mg)$, and enriched in Mg and has higher $Mg/(Mg+Fe^{2+})$ compared to the hornblende of respective host rocks (Campos, 1997; Campos *et al.*, 2002 and reference therein). Figure 5 shows that most analyzed hornblendes cluster in two groups, separated by a marked break between Si = 6.7 and Si = 6.8. The low–Si hornblende cluster (Si ≤ 6.7) shows some scatter while the high–Si hornblende cluster (Si ≥ 6.8) shows a linear relationship. That suggests a different evolution for early and late magmatic processes. The absence of intermediate analyses between the clusters may indicate rapid change in composition during magma mixing or magmatic crystallization rather than a true gap in the amphiboles, and this marks the moment at which magmatic fluid evolved to a separated phase. Consequently, the latter hornblende exhibits an oxidizing trend typified by compositions that became Mg richer with progressive crystallization (e.g. Yamaguchi, 1985, Pe-Piper, 1988). Furthermore, there is a negative correlation between Mg and $Al^{IV}$ from hornblende



Figure 3– a) Compositions of amphiboles from plutonic rocks of the Rio Espinharas hybrid complex, northeastern Brazil, according to the IMA nomenclature of Leake *et al.* (1997); b) Ca+Na+K versus Si diagram. The curved line corresponds to the limit of magmatic amphibole (Leake, 1971).
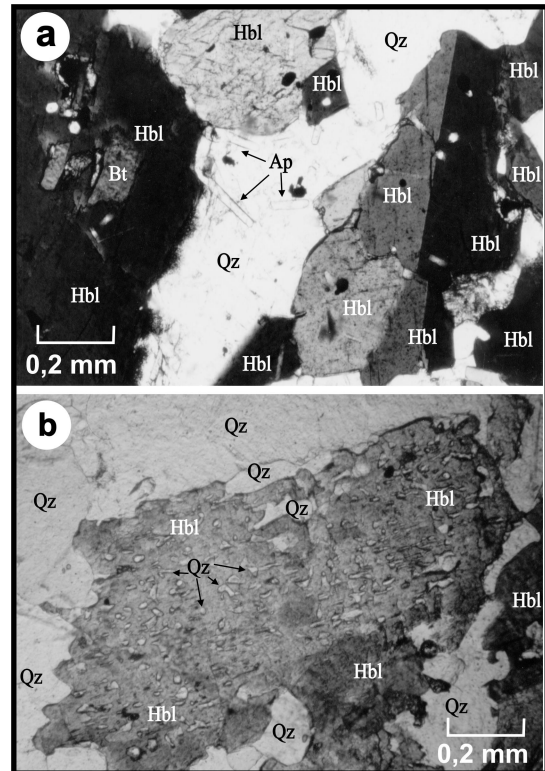
47

(*sensu lato*) to actinolite (Fig.5), and the increase in Mg/(Mg+Fe$^{2+}$) reflect increasing oxygen fugacity as the magma became more siliceous (Czamanske & Wones, 1973, Yamaguchi, 1985, Pe-Piper, 1988).

Czamanske & Wones (1973) observed that tetrahedral silicon when replaced by Al$^{IV}$ in amphibole is dominantly compensated by coupled substitution of Al$^{VI}$, Fe$^{3+}$, and Ti in octahedral–sites, and with partial occupancy of the A–site by Na and K, respectively tschermakite– and edenite–type substitutions. These coupled substitutions occur in the Rio Espinharas hybrid complex amphibole, and are illustrated by linear relationship between Al$^{IV}$ vs [(Na+K)$_A$ + (Al$^{VI}$+2Ti+Fe$^{3+}$)], and Na$_{(M4)}$ vs Ca$_{(M4)}$ (Fig.6a, b). Deficiencies in Al$^{IV}$ cations are illustrated by the data that plot below the 1:1 line (Fig.6a), and indicate that the excess in the A–site and octahedral charge is not completely compensated by the Al$^{IV}$ substitution. Therefore the linear relationships showed by substitution of Na for Ca in the M4–sites (Fig. 6b) suggest that charge balance of the excess octahedral and A–site charge is compensated by this coupled substitution in M4–sites.

Several authors (e.g. Hammarstron & Zen, 1986; Zen and Hammarstron , 988; Hollister *et al.*, 1987; Jonhson & Rutherford, 1989; Thomas & Ernst, 1990; Fershtater, 1990; Schmidt, 1992, and Anderson & Smith, 1995) suggested a geobarometer based on linear variation of aluminium content in hornblende with crystallisation pressure for rocks showing an equilibrated mineral assemblage of quartz, K–feldspar, biotite, titanite, Ti–Fe oxides, vapour and melt. The granitoids from the Rio Espinharas hybrid complex show the assemblage required to buffer Al–in–hornblende. The Fe$_{Total}$/(Fe$_{Total}$+Mg) ratios of hornblende rims in contact with quartz range from 0.4 to 0.65, excluding the sub-solidus actinolite rims. Theses values indicate relatively high **f**O$_2$ and are similar to those recommended by Anderson & Smith (1995) as ideal for application of the Al–in–hornblende geobarometer.

The relationship between tetrahedral aluminum (Al$^{IV}$) and total aluminum (Al$^{IV}$+Al$^{VI}$) of amphibole from Rio Espinharas hybrid complex is given in figure 6c. All amphibole rims show tetrahedral Al (Al$^{IV}$) within limit contents assumed for "permissible" magmatic amphibole compositions (Leake, 1971; Pe-Piper, 1988). Therefore, amphibole rim compositions are used to calculate the crystallization pressures. Actinolite rims which matle
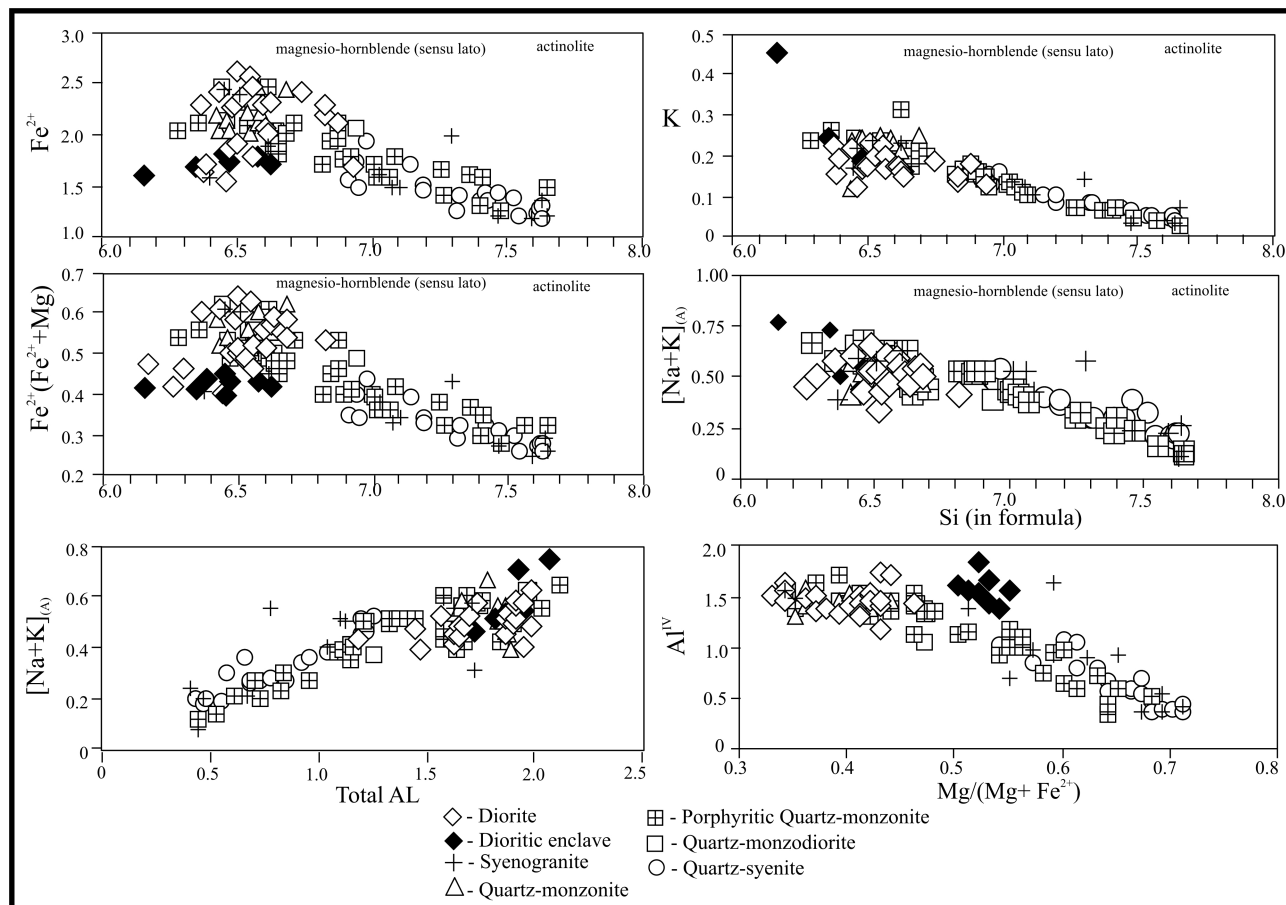


Figure 5– Variation diagrams of amphibole from granitoid rocks of the Rio Espinharas hybrid complex.
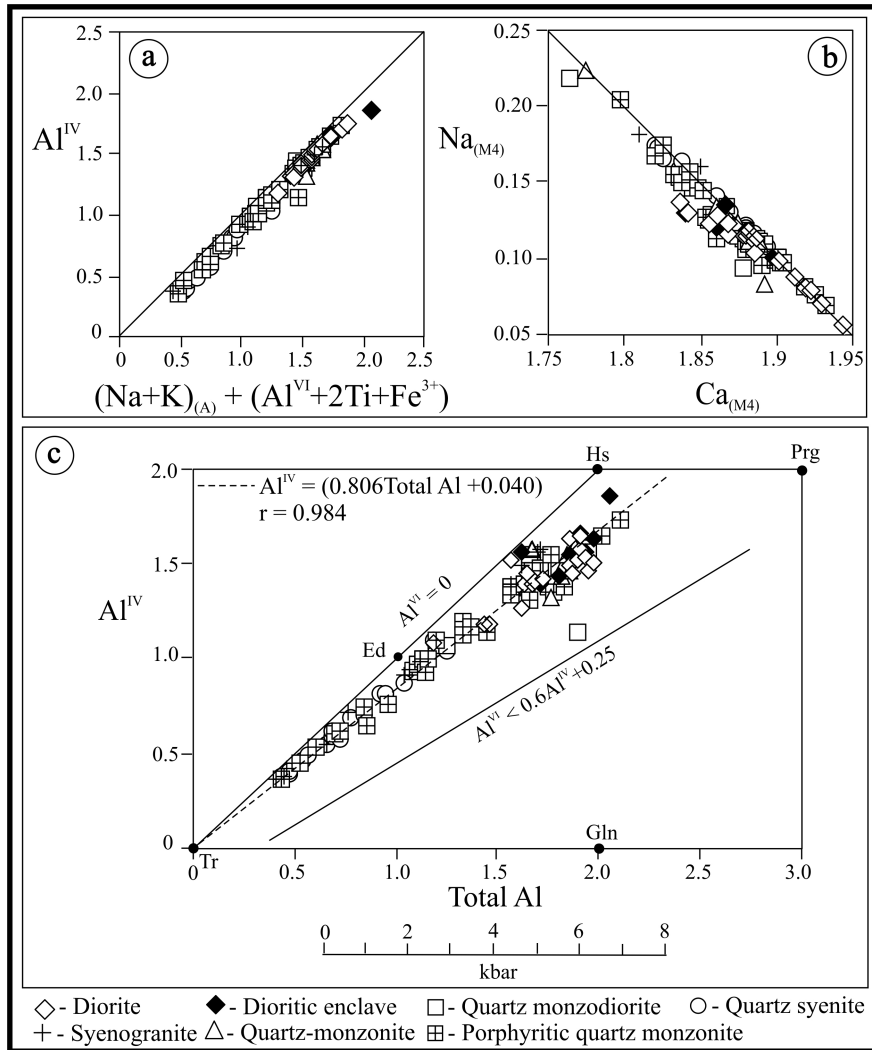
Figure 6– a) Coupled substitution diagrams of amphibole from granitoid rocks of the Rio Espinharas hybrid complex: a) $Al^{IV}$ versus $(Na+K)_{(A)} + (Al^{VI}+2Ti+Fe^{3+})$; b) $Na_{(M4)}$ versus $Ca_{(M4)}$. Trend line with 1:1 slope corresponds to ideal substitutions; c) $Al^{IV}$ versus $Al_{Total}$ diagram of amphiboles of granitoid rocks from the Rio Espinharas hybrid complex. Ideal end-member amphibole compositions: Tr: tremolite; Ed: edenite; Gln: glaucophane Hs: hastingsite; Prg: pargasite. Solid lines are proposed minimum and maximum possible values of $Al^{IV}$ in calcic amphibole (Leake, 1971). Dashed line is the linear regression on the data set, and the equation is given in the upper left corner. Approximate crystallization pressure based on the equation of Schmidt (1992) is showed.

pyroxene core were not taken into account for the pressure calculation. Pressures for low–Si amphibole range from 7.1 to 4.5 kbar, and for high–Si amphiboles range from 3.9 to 2.9 kbar (Fig.6c) were thus calculated from the Al–in–hornblende geobarometer of Schmidt (1992), calibrated to 2.5–13 kbar, temperature between 700–655 °C, with uncertainties about ± 0.6 kbar.

Under low pressure, high $fO_2$ and $PH_2O$, Si–rich amphiboles may have crystallized from magma during the late stages of solidification (Cawthorn, 1976, Yamaguchi, 1985, Pe–Piper, 1988). Pressures inferiors to 2.9 kbar as shown by high-Si amphibole from Rio Espinharas hybrid complex can be indicative of late–stage sub–solidus alteration or oxidation by exsolved fluid, which result in the growth of more magnesian and less aluminous am-

phibole (Hammarstron & Zen, 1986).

It was first suggested by Hammarstrom & Zen (1986) that Al–in–hornblende geobarometry is also temperature dependent, and later by Blundy & Holland (1990) and Holland & Blundy (1994) that the edenite content of hornblende coexisting with plagioclase is more sensitive to temperature than to pressure. Therefore, these authors proposed a new geothermometer using hornblende coexisting with plagioclase, for silica-saturated rocks equilibrated at temperature ranging from 500 to 1000 ± 40° C, and 1-15 kbar, and assemblage involving plagioclase less calcic than $An_{92}$ and amphibole containing less than 7.8 Si cations p.f.u.. It was further suggested that the Al–in–hornblende barometry would only be valid in rocks equilibrated at the same temperature. In the studied rocks, the crystallization temperatures

were calculated using the equation of Holland & Blundy (1994).

Geothermometry indicates that hornblende crystallized at **T** ranging from ca 850 to 730°C (Campos, 1997; Campos *et al.*, 2002 and reference therein). Considering the temperatures calibrated range of different geobarometers, we applied a revised expression for the Schmidt's and Johnson and Rutherford's calibrations proposed by Anderson & Smith (1995), which incorporates the effect of temperature. Taking into account the error of 0.5 to 0.6 kbar for the geobarometric methods, the new calculated pressures by the Anderson & Smith's calibration yield similar pressure to that calculated by Schimdt's method, which are 7.4 to 4.8 kbar for low–Si amphibole, and for high–Si amphiboles range from 4.3 to 3.3 kbar (Campos, 1997; Campos *et al.*, 2002 and reference therein).

## EPIDOTE PETROGRAPHY AND CHEMISTRY

The crystalline habit of epidote, with or without optic zoning and/or allanite core, is gene-

rally conditioned by available space and origin, being euhedral when included, or in contact with biotite, amphibole, or in quartz and K-feldspar aggregates, subhedral when in contact with plagioclase, and anhedral when produced by plagioclase alteration (Tulloch, 1979, 1986; Naney, 1983; Zen & Hammarstrom, 1984, 1988; Zen, 1985; Johnston & Wyllie, 1988; Bellieni *et al.* 1991; Vyhnal *et al.*,1991). The epidote from the granitoids of the Rio Espinharas hybrid complex show dimensions of up to 1 mm, and appears to be later crystallized than hornblende and earlier than biotite, which suggests a pressure crystallization ranging from 10 to 8 kbar (Schmidt & Thompson, 1996). It occurs as three primary types and one secondary (Fig.7). The pleochroic euhedral to subhedral epidote, named type–I, is dispersed and associated with mafic minerals, mainly biotite and amphibole (type–I; Fig.7a), it is never rimmed by amphibole, and rarely occurs intermingled along with other accessory minerals such as titanite, magnetite and apatite. In some cases, pleochroic euhedral to subhedral crystals of epidote are completely enveloped by biotite, and contain allanite cores (type–II; Fig.7a, b), which, in general present ave-



Figure 7– a) Zoned crystals of epidote (Ep) rimming allanite (Aln) core (I-type) partially armored by biotite (Bt) and microcline (Mc) from quartz-monzonite (XPL). Note the reaction aureole between the epidote and biotite; b) Zoned crystals of epidote rimming allanite core (II-type) armored by biotite from porphyritic quartz-monzonite (XPL); c) Zoned crystals of magmatic epidote rimming allanite core, partially armored by amphibole (Hbl) and quartz (Qz), and partially absorbed by plagioclase (Pl) (III-type) from porphyritic quartz-monzonite (PPL). Dashed lines are an attempt to reconstruct original shape of the epidote crystal indicating how much of this crystal have been corroded by the host magma; d) Secondary epidote included in plagioclase (IV-type) from quartz-syenite (PPL). Mineral abbreviation based on Kretz (1983). PPl: plane-polarized light, XPL: cross-polarized light.

50

rage dimension of about 25% of the entire crystal. Some epidote crystals shows corroded contact with plagioclase, which is interpreted as dissolution and reaction with the magma before solidification, in those portions not protected by amphibole and quartz rims (type–III; Fig.7c). Secondary anhedral epidote is rare and results from plagioclase alteration (type–IV; Fig.7d).

The textural relationships of epidote with other minerals yield information an upward magma transport (Dawes & Evans, 1991; Brandon et al., 1996). Brandon et al. (1996) considered that epidote preservation in granitic rocks from lower pressures is due to: a) fast protection of epidote from contact with the melt during low-pressure crystallization, from the armoring by mineral aggregates; or b) rapid magma ascent, which implies fast upward transport probably by dyking associated to shear zones. The textural relationship shown by epidote from granitoids of Rio Espinharas hybrid complex (Fig.7) and the geological situation of this pluton (Fig.1) are consistent with the hypothesis proposed by Brandon et al. (1996).

Brandon et al. (1996) modeled the epidote dissolution in granitic magma as function of dissolution time, crystal size, and temperature, by the equation $X = (D_{app}t)^{1/2}$ where: $\underline{X}$ is the width (mm) of the dissolved part, $\underline{D}_{app}$ is the apparent diffusion coefficient of elements (Al, Ca and Fe) between epidote and granodioritic magma at 750 $^{o}$C ($\approx 4.6 \times 10^{-17} m^2 s^{-1}$ ), and $\underline{t}$ is the dissolution time (years).

Maximum magma transport rates were estimated from the observed dissolution zone width of epidote from Rio Espinharas granitoids by using this model. In general, when in contact with plagioclase phenocrysts, type–III epidote shows resorption textures (Fig.7c). The observed dissolution zone on several epidote grains shows an average width of 0.15 mm (Fig.7c), and indicates a dissolution time span of inferiors to 14 years, at a temperature of 750 $^{o}$ C. For the porphyritic dacite dikes from the Front Range, Colorado, Dawes & Evans (1991) suggested that the preservation of 0.5 mm large epidote crystals required transport rates greater than 700 m year$^{-1}$ from 6 to 2 kbar. In turn, at $\Delta P = 2.6 \pm 0.5$ kbar, the time of 14 years required for dissolution zone of the epidote from Rio Espinharas granitoids, corresponds to an average ascent rate of 550 ($\pm$ 200) m/year. This high transport rate is similar to that estimated for fracture dyking propagation (Clemens & Mawer, 1992). Consequently, the survival of epidote in granitoids from Rio Espinharas hybrid complex can be explained by fast upward magma transport along the NNE-SSW fractures (Fig.1) associated to Brasiliano cycle (Pan-African orogeny). However, Schmidt & Thompson (1996) suggested that the existence of magmatic epidote in rocks crystallised under lower pressures can be due to magmatic crystallization under water-saturated and strongly oxidizing conditions (hematite-magnetite buffer), which expand the magmatic stability field of epidote to pressures of 3 kbar.

The epidote of granitoids from the Rio Espinharas hybrid complex has chemical compositions (Tab. 2) similar to that for magmatic epidote referred to by Vyhnal et al. (1991). When compared to those described by Farrow & Barr (1992), Sial et al. (1999), Bonzanini (2001) and Pereira (2000), they show lower contents of Si, Al, Ca and higher $Fe^{3+}$, and compared to those discussed by Bellieni et al (1991), the epidote is Si and Al depleted and rich in $Fe^{3+}$ and Ca.

The average pistacite component $[Fe^{3+}/(Fe^{3+}+Al^{VI})]$ varies according to epidote origin. The primary epidote from Rio Espinharas hybrid complex has pistacite contents between 26% in the quartz syenite and 29% in the diorite (Fig. 8), and they usually increase in single crystals from core to border (Tab. 2). The pistacite component varies independently of textural relationships among epidote and amphibole, biotite, K-feldspar or zoned epidote with allanite core. These pistacite contents are similar to those reported for typical magmatic epidote (Tulloch, 1979, 1986; Naney, 1983; Zen, 1985; Zen & Hammarstrom, 1984, 1988; Sial et al., 1999; Campos et al., 2000, 2002). The secondary anhedral epidote (type–IV) shows pistacite contents ranging from 31% to 36% (Fig.8) and usually increases in individual crystals from core to rim (Tab. 2). The type–IV epidote and the magmatic one show similar contents of Si and Mn. Pistacite component of type–IV epidote is higher than that of epidote that replaces plagioclase (Tulloch 1979, 1986; Vyhnal et al., 1991), and is similar to the epidote that replaces biotite by hydrothermal alteration (Tulloch, 1979; Zen & Hammarstrom, 1984; Zen, 1985). Farrow & Barr (1992) described primary and secondary epidote of granitoid rocks from Cape Breton whose pistacite contents vary within the range of 25 to 29%, typical for magmatic epidote (Tulloch, 1979, 1986; Naney, 1983; Zen, 1985; Zen & Hammarstrom, 1984, 1988; Vyhnal et al., 1991).

The relatively high pistacite contents ($Ps_{26}$– $Ps_{29}$) of the magmatic epidote of granitoids from Rio Espinharas hybrid complex are consistent with the

Table 2– Average electron-microprobe analyses in wt.% of epidote of plutonic rocks from Rio Espinharas hybrid complex, northeastern Brazil.

| | Magmatic Epidote | | | | | | | | | | | | Secondary Epidote | | | |
| --- | --- | --- | --- | --- | --- | --- | --- | --- | --- | --- | --- | --- | --- | --- | --- | --- |
| | Syenogranite | | Diorite | | Qz-mznt. | | Porph. Qz-mznt. | | Qz-mznd | | Quartz syenite | | Qz-mznt | | Microgranite | |
| n | 13 | 12 | 11 | 12 | 11 | 12 | 12 | 10 | 10 | 10 | 10 | 9 | 6 | 5 | 7 | 8 |
| | rim | core | rim | core | rim | core | rim | core | rim | core | rim | core | rim | core | rim | core |
| $SiO_2$ | 38,35 | 38,13 | 37,70 | 37,23 | 37,82 | 37,75 | 37,44 | 37,79 | 36,12 | 37,92 | 37,45 | 35,86 | 36,05 | 38,19 | 37,06 | 36,35 |
| $TiO_2$ | 0,06 | 0,02 | 0,06 | 0,04 | 0,08 | 0,02 | 0,04 | 0,07 | 0,01 | 0,13 | 0,01 | 0,19 | 0,16 | 0,00 | 0,04 | 0,17 |
| $Al_2O_3$ | 23,69 | 23,68 | 22,87 | 22,55 | 22,96 | 23,36 | 22,73 | 23,18 | 23,12 | 23,56 | 23,24 | 22,87 | 20,85 | 22,42 | 21,72 | 21,45 |
| $Fe_2O_3$ | 14,30 | 13,80 | 14,59 | 14,04 | 14,46 | 13,96 | 14,20 | 14,01 | 13,65 | 13,57 | 13,59 | 13,08 | 15,76 | 17,00 | 15,50 | 14,97 |
| MnO | 0,21 | 0,17 | 0,16 | 0,18 | 0,22 | 0,08 | 0,12 | 0,22 | 0,14 | 0,24 | 0,14 | 0,40 | 0,21 | 0,42 | 0,30 | 0,4 |
| MgO | 0,00 | 0,00 | 0,00 | 0,00 | 0,00 | 0,00 | 0,00 | 0,00 | — | — | 0,00 | 0,27 | 0,00 | 0,00 | 0,00 | 0 |
| CaO | 22,98 | 23,16 | 23,24 | 23,36 | 23,04 | 23,27 | 22,93 | 23,03 | 22,58 | 23,25 | 23,39 | 19,89 | 21,37 | 21,81 | 22,43 | 21,63 |
| $Na_2O$ | 0,00 | 0,03 | 0,01 | 0,00 | 0,00 | 0,02 | 0,00 | 0,00 | — | — | 0,00 | 0,55 | 0,00 | 0,04 | 0,00 | 0 |
| $K_2O$ | 0,00 | 0,02 | 0,03 | 0,00 | 0,00 | 0,00 | 0,00 | 0,01 | — | — | 0,00 | 0,03 | 0,00 | 0,01 | 0,00 | 0 |
| Total | 99,59 | 99,01 | 98,66 | 97,40 | 98,58 | 98,46 | 97,46 | 98,31 | 95,62 | 98,81 | 97,82 | 93,14 | 94,40 | 99,89 | 97,05 | 94,97 |
| *Structural formulae calculated on the basis of 12.5 oxygens.* | | | | | | | | | | | | | | | | |
| Si | 3,000 | 3,000 | 2,993 | 2,994 | 3,000 | 2,994 | 3,000 | 3,000 | 2,954 | 3,000 | 2,991 | 2,992 | 3,000 | 3,000 | 3,000 | 3,000 |
| $Al^{IV}$ | — | — | 0,007 | 0,006 | — | 0,006 | — | — | 0,046 | — | 0,009 | 0,008 | — | — | — | — |
| Σ | 3,00 | 3,00 | 3,00 | 3,00 | 3,00 | 3,00 | 3,00 | 3,00 | 3,00 | 3,00 | 3,00 | 3,00 | 3,00 | 3,00 | 3,00 | 3,00 |
| $Al^{VI}$ | 2,19 | 2,2006 | 2,1328 | 2,132 | 2,1478 | 2,1777 | 2,1525 | 2,1724615 | 2,183 | 2,194 | 2,178 | 2,241 | 2,0498 | 2,0806 | 2,074 | 2,0922 |
| Ti | 0,0035 | 0,0012 | 0,0036 | 0,0024 | 0,0048 | 0,0012 | 0,0024 | 0,0041821 | — | 0,013 | 0,00 | 0,012 | 0,01 | 0,00 | 0,002 | 0,0106 |
| $Fe^{3+}_t$ | 0,8427 | 0,8178 | 0,8716 | 0,8498 | 0,8633 | 0,8332 | 0,8572 | 0,8375426 | 0,843 | 0,814 | 0,817 | 0,821 | 0,9879 | 1,0059 | 0,945 | 0,9308 |
| Σ | 3,05 | 3,03 | 3,02 | 3,00 | 3,03 | 3,02 | 3,02 | 3,03 | 3,03 | 3,02 | 3,01 | 3,10 | 3,04 | 3,11 | 3,02 | 3,0229 |
| Mn | 0,014 | 0,011 | 0,011 | 0,012 | 0,015 | 0,005 | 0,008 | 0,015 | 0,010 | 0,013 | 0,009 | 0,028 | 0,015 | 0,028 | 0,021 | 0,028 |
| Mg | — | — | — | — | — | — | — | — | — | — | — | 0,034 | — | — | — | — |
| Ca | 1,928 | 1,954 | 1,977 | 2,013 | 1,959 | 1,977 | 1,971 | 1,960 | 1,987 | 1,972 | 2,001 | 1,778 | 1,907 | 1,837 | 1,946 | 1,915 |
| Na | — | 0,005 | 0,002 | — | — | 0,003 | — | — | — | — | — | 0,089 | — | 0,006 | — | — |
| K | — | 0,002 | 0,003 | — | — | — | — | 0,001 | — | — | — | 0,003 | — | 0,001 | — | — |
| Σ | 1,928 | 1,961 | 1,981 | 2,013 | 1,959 | 1,981 | 1,971 | 1,961 | 2,000 | 1,990 | 2,001 | 1,904 | 1,922 | 1,845 | 1,967 | 1,943 |
| $100[Fe^{3+}/(Fe^{3+}+Al^{VI})]$ | 27,79 | 27,09 | 29,01 | 28,50 | 28,67 | 27,67 | 28,48 | 27,83 | 27,37 | 26,89 | 27,27 | 26,82 | 32,55 | 32,59 | 31,30 | 30,82 |

Qz: Quartz; Porph. Qz-mznt.: Porphyritic Quartzmonzonite; n: number of analyses.

52

crystallization pressures estimated by the Al–in–hornblende geobarometer and suggest that these rocks crystallized under relatively high oxidising conditions, probably under $fO_2$ between the NNO–HM buffer curves (Liou, 1973). This high $fO_2$ is also indicated by the presence of titanite, magnetite, and by biotite compositions (Campos, 1997; Campos *et al.*, 2002).
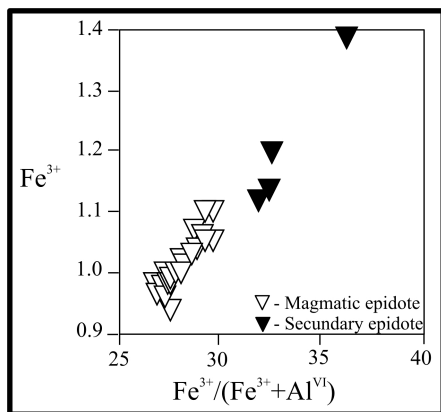


Figure 8– $Fe^{3+}$ versus pistacite contents [$Fe^{3+} / (Fe^{3+}+Al^{VI})$] on the basis of 12.5-oxygen of the epidote from granitoid rocks of the Rio Espinharas hybrid complex, north-eastern Brazil.

## PETROGENETIC IMPLICATIONS AND CONCLUSIONS

The epidote crystals that are corroded by plagioclase probably crystallized under higher pressures, at deeper levels than that of the final depth intrusion of the pluton. The corrosion of epidote and its replacement by plagioclase suggest the chemical disequilibrium of epidote, close to the final level of emplacement. These features render it probable, that epidote corrosion results from disequilibrium due to magma mixing and hybridization responsible for the genesis of studied granitoids, because the mixing process occurred at deeper levels than that of the final emplacement of the pluton (Campos *et al.*, 2002).

Textural relationships of magmatic epidote in these granitoids suggest that it crystallized simultaneously with amphibole, at pressures higher than 6 kbar. The pressures estimated by Al–in–hornblende geobarometer, in some cases, correlates with the compositional variations of coexisting epidote, that is, lower pistacite contents occur in epidote from granitoids that crystallized at high pressure, and pistacite-rich compositions occur in granitoids that crystallized at lower pressure.

The presence of preserved euhedral epidote in these granitoids, together with corroded epidote

in contact with plagioclase, reflects the fast upward magma transport ($\geq$ 550 m/y) along the NE-SW fracture system. Epidote preservation was also favored by its armoring groundmass minerals, isolating the epidote from melt. These processes occurred at low pressure and in shorter time intervals than those calculated for epidote dissolution ($\leq$ 14 years). The magmatic epidote crystals corroded by plagioclase are not equilibrated with late crystallization conditions found for the rocks of this complex (Campos, 1997, Campos *et al.*, 2002).

## REFERENCES

Anderson, J.L., Smith, D.R. 1995. The effects of temperature and fO2 on the Al-in-hornblende barometer. **American Mineralogist, 80**: 549-559.

Bellieni, G., Cavazzini, G., Fioretti, A.M., Peccerillo, A., Poli, G. 1991. Geochemical and isotopic evidence for crystal fractionation, AFC and crustal anatexis in the genesis of Rensen plutonic complex (Eastern Alps, Italy). **Chemical Geology, 92**: 21-43.

Blundy, J.D., Holland, T.J.B. 1990. Calcic amphibole equilibria and new amphibole-plagioclase geothermometer. **Contributions to Mineralogy and Petrology, 104**: 208-224.

Bonzanini, L.F. 2001. **Caracterização petrográfica, química e tecnológica de feldspatos de pegmatitos da região do Alto Potengi-RN.** Natal, 122p. Unpublished Msc thesis, Federal University of Rio Grande do Norte.

Brandon, D., Creaser, R.A., Chacko, T. 1996. Constraints on rates of granitic magma transport from epidote dissolution kinetics. **Science, 271**: 1845-1848.

Brown, G.C., Hughes, D.J., Esson, J. 1973. New XRF data retrieval technique and their application to U.S.G.S. standard rocks. **Chemical Geology 11**: 223-229.

Campos, T.F.C. 1997. **Geoquímica das rochas granitóides e seus minerais do batólito de Serra negra do Norte-RN e Rio Espinharas-PB, Nordeste do Brasil.** Porto Alegre, 408 p. Unpublished PhD thesis Federal University of Rio Grande do Sul.

Campos, T.F.C., Neiva, A.M.R., Nardi, L.S.V. 2000. Geochemistry of granites and their minerals from Serra Negra do Norte pluton, Northeastern Brazil. **Chemie der Erde, 60**: 279-303.

Campos, T.F.C., Neiva, A.M.R., Nardi, L.S.V. 2002. Geochemistry of the Rio Espinharas hybrid complex, northeastern Brazil. **Lithos, 64**: 131-153.

Cawthorn, R.G. 1976. Some chemical controls on igneous amphibole composition. **Geochimica et Cosmochimica Acta, 40**: 1319-1328.

Clemens, J.D., Mawer, C.K. 1992. Granitic magma transport by fracture propagation. **Tectonophysics, 204**: 339-360.

Cornelius, H.P. 1915. Geologische Beobachtungen im Gebiet des Forno-Gletschers (Engadin). **Centralblatt für Mineralogie Geologie und Paläontologie, 8**: 246-252.

Crawford, M.L., Hollister, L.S. 1982. Contrast of metamorphic and structural histories across the Work Channel lineament, coast plutonic complex, British Columbia. **Journal of Geophysical Research, 87** (B5): 3849-3860.

Czamanske, G.K., Wones, D.R. 1973. Oxidation during magmatic differentiation, Finnmarka Complex, Oslo Area, Norway: Part II, the mafic silicates. **Journal of Petrology, 14**: 349-380.

Dawes, R.L., Evans, B.W. 1991. Mineralogy and geothermo barometry of magmatic epidote-bearing dikes, Front Range, Colorado. **Geologial Society of America Bulletin, 103**: 1017-1031.

Dias, G., Leterrier, J. 1994. The genesis of felsic-mafic plutonic associations: a Sr Nd isotopic study of the Hercynian Braga granitoid Massif (Norther Portugal). **Lithos, 32**: 207-223.

Droop, G.T.R. 1994. Triple-chain pyriboles in Lewisian ultramafic rocks. **Mineralogical Magazine, 58**: 431-435.

Evans, B.W., Vances, J.A. 1987. Epidote phenocrysts in dacitic dikes, Boulder County, Colorado. **Contributions to Mineralogy and Petrology, 96**: 178-185.

Farrow, C.E.G., Barr, S.M. 1992. Petrology of High-Al-Hornblende and magmatic-epidote-bearing plutons in the south-eastern Cape Breton Highlands, Nova Scotia. **Canadian Mineralogist, 30**: 377-392.

Fershtater, G.B. 1990. An empirical plagioclase-hornblende barometer. **Geokhimiya, 3**: 328-335.

Gonzalez, M.G.B. 1984. **Geologia e Petrologia da área de Serra Negra do Norte-RN/PB.** Belém, 137p. Msc. Thesis. Federal University of Pará.

Hammarston, J.M., Zen, E-A.N. 1986. Aluminium in hornblende: an empirical igneous geobarometer. **American Mineralogist, 71**: 1297-1313.

Hobbs, W.H. 1889. On the paragenesis of allanite and epidote as rocks-forming minerals. **American Journal of Science, 138**: 223-228.

Holland, T., Blundy, J. 1994. Non-ideal interactions in calcic amphiboles and their bearing on amphibole-plagioclase thermometry. **Contributions to Mineralogy and Petrology, 116**: 433-447.

Hollister, L.S., Grissom, G.C., Peters, E.K., Stowell, H.H., Sisson, V.B. 1987. Confirmation of empirical correlation of Al in hornblende with pressure of solidification of calc-alkaline plutons. **American Mineralogist, 72**: 231-239.

Jardim de Sá, E.F. 1994. **A Faixa Seridó (província Borborema, NE do Brasil) e o seu significado geodinâmico na cadeia Brasiliana/Pan-Africana**. Brasília, 803p. Unpublished PhD thesis of Geosciences Institute, Federal University of Brasilia.

Johnson, M.C., Rutherford, M.J. 1989. Experimental calibration of the Al-in-hornblende geobarometer with application to Long Valley caldera (California) volcanic rocks. **Geology, 17**: 837-841.

Johnston, A.D., Wyllie, P.J. 1988. Interaction of granitic and basic magmas: experimental observations on contamination processes at 10 kbar with H2O. **Contributions to Mineralogy and Petrology, 98**: 352-362.

Keane S.D., Morrison, J. 1997. Distinguishing magmatic epidote from sub-solidus epidote: laser probe oxygen isotope composition. **Contributions to Mineralogy and Petrology, 126**: 265-274

Keyes, C.R. 1893. Epidote as a primary component of eruptive rocks. **Geological Society of America Bulletin 4**: 305-312.

Kretz, R. 1983. Symbols for rock-forming mineral. **American Mineralogist 8**:277-279.

Leake, B.E., Woolley, A.R., Birch, W.D., Gilbert, M.C., Grice, J.D., Hawthorne, F.C., Kato, A., Kisch, H.J., Krivovichev, V.G., Linehout, K., Laird, J., Mandarino, J. 1997. Nomeclature of amphiboles: report of the Subcommittee on Amphiboles of International Mineralogical Association Commission on New Mineral and Mineral Names. **Mineralogical Magazine, 61**: 295-321.

Leake, B.E. 1971. On aluminous and edenitic hornblendes. **Mineralogical Magazine, 38** (296): 389-407.

Liou, J.G. 1973. Synthesis and stability relations of epidote, $Ca_2Al_2FeSiO_{12}(OH)$. **Journal of Petrology, 14**: 381-413.

Moench, R.H. 1985. Comment and reply on "Implication of magmatic epidote-bearing plutons on crustal evolution in the accreted terrenes of Northwestern North America" and "Magmatic epidote and its petrological significance". **Geology, 14**: 188-189.

Naney, M.T. 1983. Phase equilibria of rocks-forming ferromagnesian silicates in granitic systems. **American Mineralogy, 283**: 993-1033.

Owen, J.V. 1991. Significance of epidote in orbicular diorite from the Greenville front Zone, Eastern Labrador. **Mineralogical Magazine, 23**: 35-42.

Pe-Piper, G. 1988. Calcic amphiboles of mafic rocks of the Jefferes Brooks plutonic complex, Nova Scotia, Canada. **American Mineralogist, 73**: 993-1006.

Pereira, L.S. 2000. **Geoquímica de micas e feldspatos de pegmatitos e granitos pegmatóides da região de Parelhas-RN**. Natal, 1470p. Unpublished Msc thesis, Federal University of Rio Grande do Norte.

Robinson, P., Jaffe, H.W., Ross, M., Klein-Jr, C. 1971. Orientation of exsolution lamellae in clinopyroxenes and clinoamphiboles: consideration of optimal phases boundaries. **American Mineralogist, 56**: 909-1039.

Schmidt, M.W. and Poli, S. 2004. Magmatic Epidote. **Reviews in Mineralogy and Geochemistry, 56**: 399-430.

Schmidt, M.W. and Thompson, A.B. 1996. Epidote in calc-alkaline magmas: An experimental study of stability, phase relationships, and the role of epidote in magmatic evolution. **American Mineralogist, 81**: 462-474.

Schmidt, M.W. 1992. Amphibole composition in tonalites as function of pressure: an experimental calibration of Al-in-hornblende barometer. **Contributions to Mineralogy and Petrology, 110**: 304-310.

Sial, A.N. 1990. Epidote-bearing calc-alkaline granitoid in Northeastern Brazil. **Revista Brasileira de Geociências, 20**: 88-100.

Sial, A.N., Toselli, A.J., Saavedra, J., Parada, M.A., Ferreira, V.P. 1997. Magmatic epidote-bearing granitoids in South América: Borborema province, NE Brazil, Papean Ranges, NW Argentina, and Pré-Andean to Andean magmatic arcs in Chile. In: SECOND INTERNATIONAL SYMPOSIUM ON GRANITES AND ASSOCIATED MINERALIZATIONS, 1997, Salvador, Bahia. **Extended Abstracts.** Salvador, SBG.p. 240-242.

Sial, A.N., Toselli, A.J., Saavedra, J., Parada, M.A., Ferreira,

V.P. 1999. Emplacement, petrological and magnetic characteristics of diverse magmatic epidote-bearing granitoid rocks in Brazil, Argentina and Chile. **Lithos, 46**: 367-392.

Thomas, W.M., Ernst, W.G. 1990. The aluminum contents of hornblende in calc-alkaline granitic rocks: a mineralogic barometer calibrated to 12 kbar. Fluid Mineral Interaction: a tribute to H. P. Eugster. **Geological Society Special Publication, 2**: 59-63.

Toselli, A.J., Saavedra, J., López, P. 1997. Magmatic epidote-bearing and cordierite-bearing granitoids from NW Argentina. In: SECOND INTERNATIONAL SYMPOSIUM ON GRANITES AND ASSOCIATED MINERA-LIZATIONS, 1997, Salvador, Bahia. **Excursion Guide.** Salvador, SBG.p. 70-106.

Tullock, A.J. 1979. Secondary Ca-Al Silicates as Low-grade Alteration Products. **Contributions to Mineralogy and Petrology, 69**: 105-117.

Tullock, A.J. 1986. Comments on "Implication of magmatic epidote-bearing plutons on crustal evolution in the accreted terrenes of north-western North America" and "Magmatic epidote and this petrological significance". **Geology, 14**: 186-187.

Vauchez, A., Neves, S.P., Caby, R., Corsini, M., Egydio-Silva, M., Arthaud, M.H., Amaro, V. 1995. The Borborema shear zone system**. Journal of South American Earth Science, 8**: 247-266

Vyhnal, C.R., McSween Jr., H.Y., Speer, J.A. 1991. Hornblende chemistry in southern Appalachian granitoids: implication for aluminum hornblende thermo barometry and magmatic epidote stability. **American Mineralogist, 76**: 176-188.

Yamaguchi, Y. 1985. Hornblende-Cummingtinite and Hornblende-Actinolite intergrowths from Koyma Calc-alkaline intrusion, Sussa, southwest Japan. **American Mineralogist, 7**: 980-986.

Zen, E-An. 1985. Implication of magmatic epidote-bearing plutons on crustal evolution in the accreted terrenes of northwestern North America. **Geology, 13:** 266-269.

Zen, E-An., Hammarstrom, J.M. 1988. Plumbing the depth of plutons by magmatic epidote-hornblende association: a cautionary review and an example from Round Valley pluton, Western Idaho. **Geological Society of America, Abstract with Programs, 20**: 475-476.

Zen, E-An, Hammarstrom, J.M. 1984. Magmatic epidote and its petrological significance. **Geology, 12**: 515-518.